Reaction CH3 + OH Studied over the 294−714 K Temperature and 1−100 bar Pressure Ranges

ARTICLE *in* THE JOURNAL OF PHYSICAL CHEMISTRY A · JULY 2012

Impact Factor: 2.69 · DOI: 10.1021/jp305070c · Source: PubMed

3 AUTHORS:

Manuvesh Sangwan
Carnegie Institution for Science
15 PUBLICATIONS **46** CITATIONS
SEE PROFILE

Evgeni Chesnokov
Institute Chemical Kinetics and Combustion
67 PUBLICATIONS **201** CITATIONS
SEE PROFILE

Lev N Krasnoperov
New Jersey Institute of Technology
161 PUBLICATIONS **1,295** CITATIONS
SEE PROFILE

THE JOURNAL OF PHYSICAL CHEMISTRY A

Article

pubs.acs.org/JPCA

Reaction CH_3 + OH Studied over the 294−714 K Temperature and 1−100 bar Pressure Ranges

Manuvesh Sangwan,[†] Evgeni N. Chesnokov,[‡] and Lev N. Krasnoperov*[,†]

[†]Department of Chemistry and Environmental Science, New Jersey Institute of Technology, University Heights, Newark, New Jersey 07102, United States

[‡]Institute of Chemical Kinetics and Combustion, Novosibirsk 630090, Russia

Supporting Information

ABSTRACT: Reaction of methyl radicals with hydroxyl radicals, CH_3 + OH → products (1) was studied using pulsed laser photolysis coupled to transient UV−vis absorption spectroscopy over the 294−714 K temperature and 1−100 bar pressure ranges (bath gas He). Methyl radicals were produced by photolysis of acetone at 193.3 nm. Hydroxyl radicals were generated in reaction of electronically excited oxygen atoms $O(^1D)$, produced in the photolysis of N_2O at 193.3 nm, with H_2O. Temporal profiles of CH_3 were recorded via absorption at 216.4 nm using xenon arc lamp and a spectrograph; OH radicals were monitored via transient absorption of light from a dc discharge H_2O/Ar low pressure resonance lamp at ca. 308 nm. The absolute intensity of the photolysis light inside the reactor was determined by an accurate in situ actinometry based on the ozone formation in the presence of molecular oxygen. The results of this study indicate that the rate constant of reaction 1 is pressure independent within the studied pressure and temperature ranges and has slight negative temperature dependence, $k_1 = (1.20 \pm 0.20) \times 10^{-10}(T/300)^{-0.49}$ cm^3 molecule^{-1} s^{-1}.

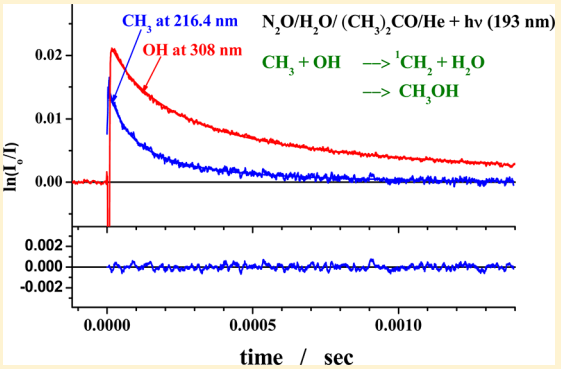

INTRODUCTION

Reaction of methyl radicals with hydroxyl radicals plays an important role in combustion chemistry.[1−3] This reaction is a multichannel reaction which proceeds via an intermediate complex.[1−3] The energetically open reaction channels are[1,2]

$$CH_3 + OH \rightarrow {}^1CH_2 + H_2O \quad (1a)$$

$$\rightarrow CH_3OH \quad (1b)$$

$$\rightarrow CH_3O + H \quad (1c)$$

$$\rightarrow CH_2OH + H \quad (1d)$$

$$\rightarrow cis\text{-}HCOH + H_2 \quad (1e)$$

$$\rightarrow trans\text{-}HCOH + H_2 \quad (1f)$$

$$\rightarrow CH_2O + H_2 \quad (1g)$$

As suggested in previous studies, channels 1a and 1b are the main reaction channels. However, relative importance of the reaction channels is temperature and pressure dependent.[4] Fockenberg et al.[5] reported that although at ambient temperature channels 1a and 1b are the major reaction channels, the relative contributions of channels 1a, 1b, 1e, and 1f at an elevated temperature (610 K) are comparable.[5] They used time-of-flight mass spectrometer connected to a tubular flow reactor. The experiments were performed at pressures of a few Torr (gas density 1.2×10^{17} molecules cm^{-3}) in helium as a bath gas. The methyl and hydroxyl radicals were produced by excimer laser photolysis (193.3 nm) of acetone and nitrous oxide in the presence of excess water or hydrogen. At 300 K the observations were consistent with singlet methylene ($^1CH_2$) and water as the main reaction products, with a small contribution of methanol formation (channel 1b). However, at about 610 K the formaldehyde isomers and methanol were formed with the yields comparable to channel 1a.

Sworski et al.[6] studied reaction 1 using flash photolysis of water vapor. Methyl radicals were produced in subsequent reaction of OH with CH_4. Methyl radicals were monitored using transient UV absorption at 216 nm. The profiles were fitted on the basis of a reaction mechanism that included several important reactions of OH, CH_3, and H species. The absolute rate constant reported was $(9.2 \pm 4.6) \times 10^{-11}$ cm^3 molecule^{-1} s^{-1}at 700 Torr and 300 K.

Anastasi et al.[7] employed pulsed radiolysis coupled with transient UV absorption at 1 bar pressure and ambient temperature. They used abstraction of H-atoms from CH_4 and H_2O by fluorine atoms in Ar/SF_6/CH_4/H_2O mixtures to generate CH_3 and OH radicals, respectively. The relative initial concentrations of CH_3 and OH radicals were controlled by

Received: May 24, 2012
Revised: July 27, 2012
Published: July 30, 2012

   dx.doi.org/10.1021/jp305070c | J. Phys. Chem. A 2012, 116, 8661−8670

varying the H_2O and CH_4 concentration ratio in the mixture. Kinetics of CH_3 was monitored at 216.4 nm. The rate constant reported in this study was $(9.4 \pm 1.3) \times 10^{-11}$ cm^3 molecule^{-1} s^{-1} at 1 bar and ambient temperature, which is in good agreement with the rate constant reported by Sworski et al.[6]

A similar approach was used by Fagerstrom et al.[8,9] to study the pressure dependence of the rate constant for reaction 1. Both CH_3 and OH radicals were monitored using transient UV absorption (at 216.4 and 309 nm, respectively). The experiments were performed over the temperature range 200−500 K and the pressure range 85−1000 mbar. The temperature dependent high pressure rate constant reported was $k_{1,\infty} = (1.44 \pm 0.15) \times 10^{-10} \exp(300/K)^{0.1}$ cm^3 molecule^{-1} s^{-1} in the temperature range 200−500 K and pressure range 85−1000 mbar.

Grotheer with co-workers[10−14] investigated the CH_3 + OH reaction using flow reactor coupled with mass-spectrometry over the pressure range 0.65−9.1 mbar and temperature range 300−700 K. Both reactants along with some products were monitored by mass spectrometry, and methyl radicals profiles served as the major observable quantity. However, at elevated temperatures a good fit was achieved only after accepting the high pressure limit rate constant of reaction 1 of 1.7×10^{-10}. At the highest temperature (700 K), the total rate constant was separated into the contributions from individual channels. The reaction channels to CH_3O + H (1c) and to CH_2OH + H (1d) were not detected. The overall rate constant was found to be pressure dependent with a high pressure association rate constant $k_{1b,\infty=}$ 1.7×10^{-10} cm^3 molecule^{-1} s^{-1}, temperature independent over the temperature range used.

Hughes et al.[15] employed laser photolysis to study reaction 1 at 290 K and 7−700 Torr pressure range. In this study excess of CH_3 relative to OH was used. Hydroxyl radicals were generated by photolysis of HNO_3 and monitored by laser induced fluorescence at 308 nm. CH_3 radicals were produced by photolysis of acetone and monitored by absorption at 216.36 nm. The pressure dependence of the rate constant was fitted using inverse Laplace transformation to obtain the microcanonical rate constant, which was incorporated in a master equation model. The rate constant determined in this study has weak pressure dependence over the 7−700 Torr pressure range. The high pressure limit rate constant reported is $(7.6 \pm 0.8) \times 10^{-11}$ cm^3 molecule^{-1} s^{-1}.

Pereira et al.[1] measured the rate constants of the CH_3 + OH reaction using laser flash photolysis combined with laser induced fluorescence at temperatures 290, 473, and 700 K over the pressure range 7.6−678 Torr. Photolysis of acetone and traces of water at 193 nm produced CH_3 and OH radicals simultaneously; the concentration of CH_3 was kept in large excess of the OH concentration. Laser induced fluorescence was used for monitoring of OH radical, whereas CH_3 radical was monitored by UV absorption at 216.4 nm. The data analyzed using master equation and the inverse Laplace transform resulted in the high pressure limit rate constant $k_{1,\infty} = (8.0 \pm 0.3) \times 10^{-11}(T/300\ K)^{-0.79\pm0.09}$ cm^3 molecule^{-1}s^{-1}. A moderate pressure dependence of the rate constant over the experimental (7.6−678 Torr) pressure range was observed, as well as a slightly negative temperature dependence in the range 298−710 K.

Deters et al.[16] studied reaction 1 at ambient temperature over the pressure range 0.7−467 mbar using laser photolysis−transient absorption (45−467 mbar) and discharge flow−laser magnetic resonance techniques (0.7−4 mbar). At higher pressures, the pressure independence of the overall rate constant of reaction 1 was observed, whereas over the low pressure range the rate constant increased slightly with pressure and approached the high pressure value obtained from the laser flash photolysis with transient UV absorption spectrometry experiments. The branching ratio of channel 1a and the overall reaction rate was determined as 0.89 at pressure 1.3 mbar and 298 K.

Reaction 1 was also studied at high temperatures using shock tubes. Bott and Cohen[17] studied reaction 1 at 1200 K and 1 atm pressure. Thermal dissociation of *tert*-butyl hydroperoxide in the shock wave was used for simultaneous production of OH and CH_3 radicals. The decays of OH radicals were monitored by UV absorption at ca. 309 nm. The rate constant reported is $(1.8 \pm 0.50) \times 10^{-11}$ cm^3 molecule^{-1} s^{-1} at 1 atm and 1200 K.

Krasnoperov and Michael[18] used shock tube coupled with a multipass absorption cell to study the CH_3 + OH reaction and the thermal dissociation of CH_3OH. The rate constant obtained was $1.74 \times 10^{-11} \exp(915\ K/T)$ over the temperature range 834−2383 K and the pressure range 50−940 Torr. Thermal decomposition of *tert*-butyl hydroperoxide, di-*tert*-butyl peroxide, methanol, and methanol iodide were used as pyrolytic precursors of hydroxyl and methyl radicals. A similar reflected shock tube study performed later using a White multipass absorption cell with 56 passes (total path length of 4.9 m) for monitoring of OH radical at 308 nm by Srinivasan et al.[19] resulted in a rate constant of $(1.3 \pm 0.2) \times 10^{-11}$cm^3 molecule^{-1} s^{-1} in the 1000−1200 K temperature range, about a factor of 3 lower than that reported by Krasnoperov and Michael.[18]

Most recently, reaction 1 has been studied at high temperatures by Vasudevan et al.[20] using a shock tube. In this study, azomethane and methyl iodide served as a source of CH_3 radicals and *tert*-butyl hydroperoxide was used as a source for OH radicals. The overall rate constant was measured in the temperature range 1081−1426 K. The rate constant reported in this study (2.98×10^{-11} at 1192 K) is in excellent agreement with the earlier study of Krasnoperov and Michael,[18] and a ca. factor of 3 higher than that reported by Srinivasan et al.[19]

Reaction 1 was extensively studied theoretically.[2,21−23] Jordan et al.[23] performed canonical variational transition state (cVTS) theory calculations using an extended Gorin model. The calculated high pressure limit association rate constant is $1.72 \times 10^{-10}(T/300\ K)^{0.27}$ cm^3 molecule^{-1} s^{-1} with a weak positive temperature dependence.

Xia et al.[2] characterized the potential energy surface of the CH_3OH system by ab initio molecular orbital theory calculations at the G2M level of theory. The rate constant for CH_3 + OH was calculated using variational RRKM theory and compared with the available experimental data. They concluded that the bimolecular reaction of CH_3 and OH, the total rate constant, and the relative branching ratios of the $^1CH_2$ + H_2O and H_2 + HCOH channels at lower pressures (P < 5 Torr) could be reasonably accounted for by the theory. For the reaction of $^1CH_2$ with H_2O, both the yield of CH_3 + OH and the total rate constant could also be satisfactorily predicted theoretically. The production of $^3CH_2$ + H_2O by the singlet to triplet surface crossing was neglected in the calculations. The predicted high pressure rate constant $k_{1,\infty}(298\ K) = 2.2 \times 10^{-10}$ cm^3 molecule^{-1} s^{-1} with a small negative temperature dependence.

Ing et al.[21] calculated the pressure- and temperature-dependent rate constant of reaction 1 using quantum RRK

theory combined with the master equation analysis for the pressure falloff. They predicted the high pressure rate constant of (1) of 1.5×10^{-11} with a positive temperature dependence over the 300−2500 K temperature range.

In a recent theoretical study, Jasper et al.[22] used a microcanonical two-state model to describe the association rate constant over a broad temperature range as well as the master equation simulations for the pressure dependence of the rate constant of reaction 1. They predicted that the reaction is close to the high pressure limit at 298 K at 1000 Torr, the variation of the rate constant over the pressure range 200−1000 Torr is ca. 15%. The computed high pressure limit rate constant at ambient temperature (9.82×10^{-11}) agrees well with the rate constant reported by Sworski et al.[6] and Anastasi et al.[7] They reported very small negative temperature dependence of $k_{1,\infty}$ (ca. 9% decrease over the temperature range 300−2500 K).

Despite the large number of experimental studies on the reaction of CH_3 with OH, there is no experimental data on the pressure dependence of this reaction at elevated pressures and temperatures. All previous experimental studies have been performed at low to moderate pressures (0.0006−5 bar). In addition, there is still significant discrepancy in the absolute rate constants as well as in the temperature dependence at ambient as well as elevated temperatures. These were the motivations for the current study.

EXPERIMENTAL SECTION

Experimental Setup. The experimental setup is described in detail elsewhere;[24−26] therefore, only a brief description critical for the current experiments is given here. The approach is based on the excimer laser photolysis coupled to UV−vis transient absorption spectroscopy and to a high-pressure flow system. Helium was used as a bath gas in all experiments. The measurements were performed over the 1−100 bar pressure and 21−441 °C temperature ranges. A detailed description of the heatable high-pressure flow reactor employed in this study is given in our previous works.[25,27] Two UV-grade quartz windows (12.7 diameter, 9.5 mm thick) were sealed at the end of the reactor at ambient temperature outside the high-temperature zone using Viton O-rings. The preheated reactant mixture entered the reactor tube in the center and left through the two outlets located on two sides 5 cm away from the center but within the uniform temperature zone. Additional flows of the bath gas (He) entered the reactor near the windows to flush gas from the windows toward the outlets. Two additional thick (9.5 mm) quartz windows, separated by a stainless steel insert, were placed without sealing inside the reactor near the reactor outlets. This "four windows" configuration prevented penetration of the reactants out of the observation zone, provided precise definition of the observation zone within the uniform temperature region and allowed avoiding of windows sealing at elevated temperatures. The length of the insert determined the optical path in the zone of reactants of 10.13 cm. To achieve uniform concentration profiles across the reactor cross-section, the laser beam was formed using a spherical lens (f = +30 cm, the distance from the reactor center 82 cm) and a cylindrical lens (f = +30 cm, the distance from the reactor center 35 cm). The beam profile was measured by scanning with a small hole diaphragm (ca. 0.5 mm) combined with an energy meter. The beam uniformity across the reactor cross-section was ±7.3% from the mean value. More details of the experimental arrangements and the signal accumulation are described elsewhere.[24−27] The gas flow rates were controlled by high pressure mass flow controllers (Brooks, model 5850). The total flow rates of the reactant mixtures with helium were in the range 360−4500 sccm (standard cubic centimeters per minute). Additional flush flows to the cold reactor windows were in the range 270−600 sccm.

Acetone−water mixtures were carefully degassed before loading in the stainless steel syringe. The mole fraction of acetone in water was varied from 0.02 to 0.04. Acetone−water mixtures were injected into the evaporator of the high pressure flow system using a precision syringe pump (Harvard Apparatus, Model PHD 4400) through a capillary tube. The temperature of the evaporator was kept at 90 °C, it was observed that this approach produces steady and stable flows of acetone−water mixtures over the pressure range 1−100 bar. The flow rate of acetone−water mixtures was varied in the range of 0.5−10 μL/min depending upon the reactor pressure and temperature. The concentrations of the precursors used: $(0.4−1.7) \times 10^{17}$ molecules cm^{-3} for N_2O, $(0.93−14.6) \times 10^{15}$ for CH_3COCH_3, and $(1.4−7.0) \times 10^{17}$ for H_2O. The laser photon fluence inside the reactor was varied in the range $(2.4−11) \times 10^{15}$ photons cm^{-2} $pulse^{-1}$. The initial concentrations of hydroxyl radicals were in the range $(5−22) \times 10^{13}$ molecules cm^{-3}. The pressure range was 1−100 bar (He), the temperature range was 295−714 K. The highest temperature was limited by the thermal stability of the precursors. The concentrations of the radicals precursors were monitored downstream the reactor by an online quadrupole mass-spectrometer (Finnigan 4021) at m/z = 43, 44 for N_2O, m/z = 58 for acetone, relative to the signal of argon added to the mixture (0.001% of argon, m/z = 40).

Noticeable depletion of the radical precursors (acetone and nitrous oxide) was observed above 714 K, probably due to a heterogeneous reaction of these species on the preheating tubing and reactor walls. These experiments are illustrated in Figure 1. The two reactants separately are stable over the whole accessible temperature range (295−834 K); however, when mixed together, they react at temperatures above 714 K.

The repetition rate of the laser was set to ensure complete replacement of the gas mixture in the reactor between the pulses (0.1−4 Hz depending upon the reactor pressure).

In Situ Actinometry. One of the most important requirements in studying the radical−radical reactions is reliable determination of the absolute concentrations of free radicals. To determine radical concentration accurately, it is necessary to know the photon fluence inside the reactor (Table 1). In this work, the absolute concentrations of OH and CH_3 radicals were determined on the basis of the photon fluence inside the reactor, the absorption cross sections of N_2O and acetone at 193.3 nm, and the efficiency of conversion of $O(^1D)$ atoms produced in the photolysis of N_2O to OH radicals. The latter was typically ca. 0.79 × 2 and was accurately evaluated using a small reaction mechanism (Table 2). The absorption cross-section of N_2O is accurately known at 298 and 1 bar. At other conditions, the cross sections of N_2O were measured in previous work.[27] The absorption cross section of acetone was determined in this study (Supporting Information). The major source of errors is in the determination of the laser light intensity inside the reactor. Outside laser energy meters require calibrations; in addition, window transmittance drift due to film deposition caused by contaminations introduces additional errors. In this work, we used an in situ laser light actinometry based on the stable molecule formation with very well characterized cross-section at a monitoring wavelength.

dx.doi.org/10.1021/jp305070c | J. Phys. Chem. A 2012, 116, 8661−8670

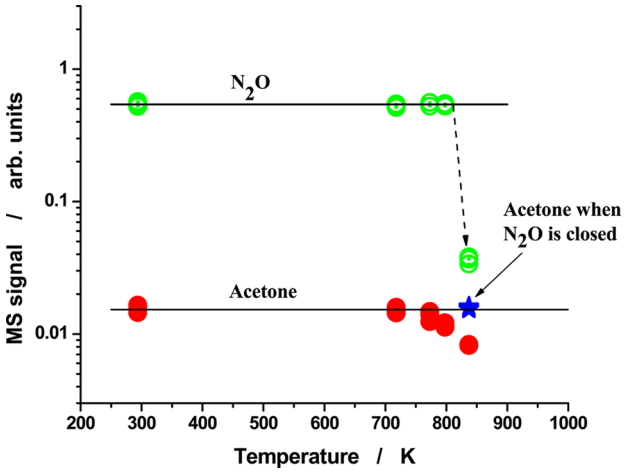

Figure 1. Thermal stability of the precursors (N_2O and acetone). The precursors were measured downstream from the reactor using an online quadrupole mass-spectrometer at m/z = 43, 44 for N_2O, m/z = 58 for acetone, relative to the signal of argon added to the mixture (0.001% of argon, m/z = 40). N_2O flow rate = 1.5 sccm, acetone = 0.033 sccm, total flow rate = 450 sccm, p = 1 bar (He). Key: open circles, N_2O; closed circles, acetone; filled stars, the signal of acetone when the flow of N_2O is closed. Note different MS sensitivities for acetone and N_2O.

Specifically, ozone formation, monitored at 253.7 nm, in the photolysis of $N_2O/O_2/N_2$ mixtures at 1 bar and 298 K, was used. Details of this technique can be found in our previous work.[27]

Usually, two such determinations were performed, before and after a series of measurements. Simultaneously, the readouts of the pyroelectric detector measuring laser pulse energy after the reactor were recorded.[27] The readouts of the pyroelectric detector in the kinetic measurements were used then to introduce proper corrections for the drift of the laser energy during a series of experiments.

Reagents. In the initial experiments UHP grade helium (99.9995%) from Airgas passed through an in-line oxygen trap (R&D Separations, Model OT2-SS, manufacturer stated oxygen content reduction to 15 ppb) was used. Later, it was replaced with BIPHelium from Airgas with 99.9999% purity with reduced oxygen content (<10 ppb). Pure nitrous oxide was obtained from Scott Specialty Gases (99.9995%). In the high pressure experiments, certified mixture of N_2O in He (mole fraction of 0.025, the accuracy ±2%) obtained from Matheson Tri-Gas, was used. Purified water (Milli-Q) with TOC less than 5 ppb) was degassed by using three freeze–pump–thaw cycles and used as a reactant supplied by a syringe pump (Harvard Apparatus PHD4400) as well as in the low pressure H_2O/Ar discharge hydroxyl monitoring lamp. Acetone used in the acetone–water mixtures was purchased from Fisher Scientific (99.7%). UHP Ar obtained from Matheson TriGas (99.999%) was used in the H_2O/Ar lamp.

OH and CH_3 Radicals Generation and Monitoring. OH radicals were generated in pulse photolysis of N_2O in the presence of water at 193.3 nm (ArF excimer laser):

$$N_2O + h\nu(193\text{nm}) \rightarrow O(^1D) + N_2 \quad \text{(P1a)}$$

$$\rightarrow N(^4S) + NO(^2\Pi) \quad \text{(P1b)}$$

$$O(^1D) + H_2O \rightarrow 2OH(v = 0, 1, 2) \quad \text{(2a)}$$

$$\rightarrow O(^3P) + H_2O \quad \text{(2b)}$$

$$\rightarrow H_2 + O_2 \quad \text{(2c)}$$

The quantum yield of the major channel P1a is unity within 1%, the minor channel P2b is less than 0.8%.[28] The yield of vibrationally excited hydroxyl radicals OH(v = 1, 2) formed in the reaction of $O(^1D) + H_2O$ (reaction 3a) is 22–32%.[29−32] A fraction of $O(^1D)$ formed in photolysis of N_2O reacts with N_2O:

$$O(^1D) + N_2O \rightarrow NO + NO \quad \text{(3a)}$$

$$\rightarrow O_2 + N_2 \quad \text{(3b)}$$

$$\rightarrow O(^3P) + N_2 \quad \text{(3c)}$$

The kinetics of hydroxyl radical decay was monitored by absorption in the UV (multiline at ca. 308 nm). A low pressure resonance a hydroxyl lamp was employed. The emission spectrum of the OH radical consists of a large number of narrow rotational lines grouped around 308 nm. The relative intensity as well as the width of the absorption lines depends on the reactor temperature and pressure. Consequently, the apparent absorption cross-section of hydroxyl is also pressure and temperature dependent. For the purposes of the data interpolation and evaluation of the "curve of growth", a spectroscopic model was built.[27] The detailed description of the low pressure lamp and the spectroscopic model can be found in our previous work.[27]

Photolysis of acetone at 193.3 nm was used to produce CH_3 radicals. There are two other possible channels in the photolysis of acetone at this wavelength:

$$(CH_3)_2CO + h\nu(193\text{nm}) \rightarrow 2CH_3 + CO \quad \text{(P2a)}$$

$$\rightarrow CH_2COCH_3 + H \quad \text{(P2b)}$$

$$\rightarrow CH_4 + CH_2O \quad \text{(P2c)}$$

Lightfoot et al.[33] measured the quantum yields of different channels in photolysis of acetone at 193.3 nm. They determined ϕ_{P2a}= 0.95, ϕ_{P2b} = 0.03, and ϕ_{P2c} = 0.02 at 300 K with a negligible temperature dependence (over the 300–600 K temperature range).

The decay of methyl radicals was monitored by absorption at 216.4 nm (1200 groove/mm grating, 300 mm focal distance, both slits 0.25 mm, triangle slit function, fwhm = 0.64 nm) using xenon arc lamp combined with an imaging spectrometer (Acton 300i).

RESULTS AND DISCUSSION

Transient absorption profiles of OH and CH_3 were measured at 46 combinations of temperature and pressure (Table 1). Sample absorption temporal profiles at 308 and 216 nm are shown in Figure 2. To determine the rate constant of reaction 1, a reaction mechanism (Table 2) was used to model and fit the experimental profiles. Absorption profiles were fitted by numerical solutions of a system of differential equations corresponding to the reaction mechanism using SCIENTST software.[34]

dx.doi.org/10.1021/jp305070c | J. Phys. Chem. A 2012, 116, 8661–8670

Table 1. Experimental Conditions and the Rate Constants of Reaction 1[a]

p/bar (He)	T/K	$[N_2O]_0/10^{16}$	$[H_2O]_0/10^{17}$	$[(CH_3)_2CO]_0/10^{15}$	photon fluence/10^{15} photon cm^{-2}	no. density/10^{20}	$[CH_3]_0/10^{13}$	$[O(^3P)]_0/10^{11}$	$[NO]_0/10^{12}$	$[OH]_0/10^{13}$	$k_1/10^{-11}$/cm^3 molecule^{-1} s^{-1}
1.01	296	9.68	3.95	1.90	3.67	0.248	4.76	1.75	4.27	5.30	12.8
1.01	297	9.50	3.87	0.93	4.13	0.243	2.26	1.93	4.71	5.87	12.4
1.01	298	9.43	3.85	1.85	4.23	0.242	5.36	1.96	4.80	5.99	12.7
1.01	355	8.03	3.28	1.57	3.64	0.206	4.67	1.73	4.22	5.26	12.2
1.01	355	7.87	3.21	1.54	4.21	0.202	5.30	1.96	4.78	5.97	10.5
1.01	414	6.87	2.80	1.35	3.39	0.176	4.28	1.64	4.0	4.90	11.6
1.01	497	5.73	2.34	1.12	3.56	0.147	4.12	1.69	4.12	5.15	9.22
1.01	555	5.03	2.05	0.987	4.04	0.129	4.34	1.87	4.59	5.72	9.08
1.01	588	4.85	1.97	0.950	3.65	0.124	3.88	1.73	4.24	5.28	7.63
1.01	626	4.46	1.81	0.875	3.93	0.114	3.93	1.82	4.46	5.56	7.98
1.01	669	4.17	1.70	0.818	3.98	0.107	3.82	1.85	4.52	5.64	6.82
1.01	669	4.24	1.71	0.830	3.16	0.108	2.67	1.49	3.65	4.55	6.07
1.01	714	3.91	1.59	0.767	4.08	0.10	3.73	1.89	4.63	5.77	5.83
2.91	298	12.6	3.10	2.47	5.82	0.730	3.25	3.25	7.95	9.92	11.5
2.91	294	12.8	3.10	0.752	6.16	0.730	3.85	3.85	14.1	10.5	12.2
2.91	298	12.2	3.44	7.11	11.2	0.710	59.3	13.0	23.0	19.1	12.2
2.91	355	10.2	2.86	5.92	9.51	0.590	48.1	11.0	19.3	16.0	11.8
2.91	414	8.78	2.47	5.11	10.9	0.510	54.6	12.8	22.5	18.6	12.1
2.91	555	6.88	1.93	4.01	10.2	0.399	50.9	12.6	22.2	18.3	11.5
2.91	626	5.81	1.63	3.38	10.5	0.337	43.6	11.9	21.9	18.0	11.0
2.91	669	5.43	1.52	3.15	9.46	0.314	36.1	10.4	18.4	16.1	10.3
2.91	714	5.09	1.43	2.96	8.87	0.295	36.6	11.1	19.6	15.1	9.22
9.84	297	11.3	3.61	1.74	4.84	2.40	5.27	2.71	8.06	7.88	12.1
9.88	355	9.40	3.0	1.44	5.03	1.99	2.81	2.81	8.37	8.18	9.05
9.84	355	11.3	3.61	1.74	4.03	2.40	2.71	2.71	8.06	7.88	12.1
9.84	414	8.05	2.57	1.24	4.95	1.71	5.05	2.76	8.24	8.05	10.2
9.88	414	8.05	2.56	1.24	4.95	1.70	5.05	2.76	8.24	8.05	10.2
9.84	497	6.64	2.10	1.02	4.90	1.40	4.57	2.70	8.03	7.85	9.62
9.84	555	6.01	1.91	0.924	4.90	1.27	4.36	2.73	8.14	7.96	8.0
9.84	555	6.02	1.91	0.924	4.90	1.27	4.36	2.74	8.15	7.96	8.0
9.84	588	5.61	1.79	0.862	4.90	1.19	4.19	2.72	8.09	7.85	6.89
9.84	626	5.27	1.68	0.81	4.94	1.12	4.04	2.73	8.13	7.94	9.06
9.84	669	4.92	1.56	0.754	4.50	1.04	3.32	2.48	7.38	7.21	6.77
29.9	294	15.9	6.76	1.59	4.86	7.28	6.70	3.84	9.16	11.8	12.3
29.9	298	15.5	7.03	14.6	6.65	7.19	106.4	6.72	11.6	16.1	12.5
29.9	355	12.9	5.86	12.1	7.10	5.99	99.1	7.18	12.4	17.2	10.8
29.9	414	11.1	5.03	10.4	7.10	5.14	89.9	7.25	12.5	17.3	11.5
29.9	555	8.28	3.77	7.82	9.26	3.85	93.6	9.50	16.4	22.5	10.8
29.9	626	7.24	3.30	6.85	8.60	3.37	76.7	8.71	15.0	20.6	6.16
29.9	669	6.87	3.13	6.49	8.54	3.20	73.7	8.79	15.2	20.8	5.91
29.9	714	6.44	2.94	6.09	8.25	3.0	67.2	8.51	14.7	20.1	9.01
101	294	16.9	4.37	2.0	6.25	23.5	22.3	5.57	19.6	15.4	11.9
101	414	12.2	3.12	1.45	4.61	16.8	12.5	4.19	14.7	11.6	7.79
101	555	9.14	2.34	0.551	5.23	12.6	4.84	4.78	16.8	13.2	7.68
101	626	8.14	2.10	0.492	5.28	11.3	4.17	4.84	17.0	13.4	11.1
101	669	7.61	1.95	0.922	5.20	10.5	7.36	4.76	16.7	13.2	8.49

[a]All concentrations in molecules cm^{-3}.

The UV absorption cross sections and the rate constants, used in the fits, were either measured in the current work (absorption cross sections of acetone and CH_3) or were taken from the literature and from our previous work.[27] The reaction mechanism and the kinetic parameters used in the model are listed in Table 2. The decay of OH and CH_3 radicals is almost entirely controlled by reaction 1 as well as self-reactions of these radicals (reactions 5 and 7). Several other reactions also contribute into the decay rate. At typical experimental conditions (Table 1), the total contributions of all other reactions into the rate constant of reaction 1 returned from the fits is about 1% at 1 bar both at ambient temperature and at 714 K. At 100 bar the contribution is ca. 15% at ambient temperature and ca. 8% at 669 K. The rest of the reactions in the mechanism were considered to elucidate their potential role as well as to introduce these small corrections. Several of them play only a marginal role (if any) under the conditions of the current study.

dx.doi.org/10.1021/jp305070c | J. Phys. Chem. A 2012, 116, 8661−8670

Table 2. Reaction Mechanism Used To Fit the Experimental Profiles

reaction	reactants	products	rate constant[a]	reference	comment	relative maximum rate[b]
1a	$OH + CH_3$	$H_2O + {}^1CH_2$	to be determined			1.00
1b		CH_3OH				
2a	$O(^1D) + H_2O$	2OH	$1.7 \times 10^{-10} \exp(36/T)$	41		
2b		$H_2 + O_2$	2.2×10^{-12}	42		
2c		$O(^3P) + H_2O$	$<0.003k_{3a}$	43	neglected	
3a	$O(^1D) + N_2O$	2 NO	8.37×10^{-11}	branching ratio of 0.62 based on ref 42	The total rate constant $k_2 = 1.35 \times 10^{-10}$ is the average of three studies[43−45] as discussed by Bahng and Macdonald.[46]	
3b		$N_2 + O_2$	5.13×10^{-11}	branching ratio of 0.38[42]		
3c		$O(^3P) + N_2O$	1.3×10^{-12}	41	$k_{2c}/k_2 < 0.01$,[41] set to 1.3×10^{-12}	
4	$O(^1D) + CH_4$	$OH + CH_3$	1.3×10^{-10}	47		
5a	$OH + OH$	$H_2O + O$	$7.1 \times 10^{13} \exp(210K/T)$	48	lit. for $T < 415$ K, Troe fit above 414 K[27]	0.05
5b		H_2O_2	$k_{Sb,\infty} = (2.4 \pm 0.6) \times 10^{-11}(T/300)^{-0.5}$; $k_{Sb,0} = [He](9.0 \pm 2.2) \times 10^{-31}(T/300)^{-3.5\pm0.5}$; $F_{c=0.37}$	27		0.08
6	$OH + CH_4$	$H_2O + CH_3$	$4.16 \times 10^{-13}(T/298)^{2.18} \exp(-1232/T)$	49		3×10^{-7}
7	$CH_3 + CH_3$	C_2H_6	this work		separately determined for specific temperatures and pressures (see text)	0.16
8	$OH + O$	$O_2 + H$	$2.4 \times 10^{-11} \exp(110/T)$	42		4.5×10^{-3}
9a	$OH + H$	$H_2 + O$	$6.86 \times 10^{-14}(T/298)^{2.8} \exp(-1950/T)$	50		4×10^{-8}
9b		H_2O	[M] $1.6 \times 10^{-31}(T/298)^{-2.6}$	51		0.18
10	$CH_3 + O$	$H_2CO + H$	1.4×10^{-10}	52		6.1×10^{-3}
11	$OH + NO$	HONO	$k_{11,0} = 6.0 \times 10^{-31}(T/300)^{-2.5}$; $k_{11,inf} = 3.3 \times 10^{-11}(T/300)^{-0.3}$; $F_{11,cent} = 0.60 \exp(91/T)$	53	$F_{11,cent}$: fit of the data from ref 53	0.07
12	$CH_3 + H$	CH_4	$6.2 \times 10^{-29}(T/298)^{-1.8}$	1		0.06
13	$OH + CH_2$	$CH_2O + H$	3×10^{-11}	54		0.06
14	$OH + (CH_3)_2CO$	$CH_3CH_2CO + H_2O$	$3.15 \times 10^{-14}(T/300)^4 \exp(453/T)$	55		0.03
15	$OH + H_2O_2$	$H_2O + HO_2$	$2.9 \times 10^{-12}\exp(109/T)$	56		4.0×10^{-4}
16	$OH + HO_2$	$H_2O + O_2$	$4.8 \times 10^{-11} \exp(250/T)$	57		1.5×10^{-4}
17	$HO_2 + NO$	$OH + NO_2$	$4 \times 10^{-12} \exp(223/T)$	58		4.1×10^{-6}
18	$CH_3 + NO$	CH_3NO	$2.1 \times 10^{-30}(T/298\ K)^{-1.87}$	59		0.011
19	$CH_3 + H_2O_2$	$CH_4 + HO_2$	$2 \times 10^{-14} \exp(300/T)$	54		3.2×10^{-6}

[a]Rate constants and concentrations unit based on molecule, cm^3, and s. [b]Maximum reaction rate relative to the maximum (initial) total rate of reaction 1 (1a + 1b), for the experimental conditions at 294 K, 100 bar, $[CH_3]_0 = 7.32 \times 10^{13}$, $[OH]_0 = 1.54 \times 10^{13}$ molecules cm^{-3} (other relevant concentrations are listed in Table 1).

dx.doi.org/10.1021/jp305070c | J. Phys. Chem. A 2012, 116, 8661−8670

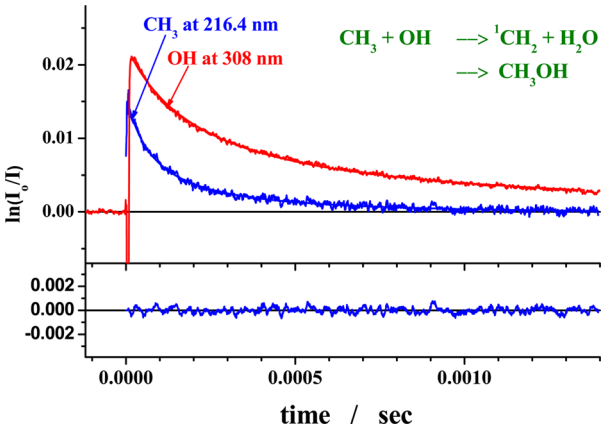

Figure 2. Sample temporal profiles of OH and CH_3 decay. Solid lines: fits by the reaction mechanism (see text). The residual is shown for CH_3 absorption. Pressure = 1 bar (He), temperature = 298 K, $[CH_3] = 5.3 \times 10^{13}$, $[OH] = 5.9 \times 10^{13}$, $[N_2O] = 7.9 \times 10^{16}$, $[(CH_3)_2CO] = 1.85 \times 10^{15}$ molecules cm^{-3}.

Reactions of $O(^1D)$ (reactions 2−4, Table 2) are fast and the time required for these reactions completion (typically 10^{-8} s) is very short comparable to the lifetimes of other transient species. Therefore, in the kinetic modeling these reactions were treated separately. The role of these reactions is to produce the initial concentrations of OH radicals as well as small concentrations of NO, O, and H, whose subsequent reactions are taken into account in the reaction mechanism. The initial concentrations of these species were calculated on the basis of the rate constants and branching ratios of reactions 2−4. The transient species in the kinetic modeling were OH, O, NO, CH_3, H, CH_2, HONO, H_2O_2, and HO_2. The concentrations of N_2O, H_2O, and $(CH_3)_2CO$, which are present in large excess of the transient species (30−4000 times), were considered to be constant during the course of the reaction. Photolysis of water ($\sigma_{H_2O}(193.3) = 1.51 \times 10^{-21}$ cm^2 $molecule^{-1}$ [27]), although it contributes to the initial concentrations of hydroxyl, when taken into account does not contribute more than 0.5% to the returned rate constants for reaction 1 at ambient temperature and 1 and 100 bar pressures, and maximum of 2% at the highest temperature at 1 and 100 bar pressure; therefore, it was neglected. This is caused by only a minor role played by hydrogen atoms in the reaction mechanism, the absolute concentrations of hydroxyl radicals are accounted explicitly in the fits. The initial concentrations of CH_2, HONO, H_2O_2, and HO_2 were set to zero.

The wall loss of hydroxyl radicals on the wall material (stainless steel) is efficient and is diffusion controlled. In the worst situation (1 bar, 714 K) the contribution of the wall loss to the total loss rate of hydroxyl radicals is only ca. 4%. Moreover, it is not relevant in this study, as we used explicit concentration temporal profiles of OH in the processing of the methyl radical profiles. The wall loss rate constant of methyl radicals does not exceed the diffusion controlled rate constant, $5.784\ D_{CH_3-He}/R^2$. The diffusion coefficient of CH_3 in He was evaluated as $D_{CH_3-He} = D_{CH_3-He,298}(T/298\ K)^{1.5}$. The room temperature value of $D_{CH_3-He,298} = 905$ Torr cm^2 s^{-1} = 1.19 bar cm^2 s^{-1} was taken from the literature.[35,36] With the reactor insert internal radius of 0.38 cm, at the highest temperature of 714 K this results in $k_{w,OH} < 177$, 59, and 18 s^{-1} for 1, 3, and 10 bar, respectively. The largest contribution of the wall loss to the decay rate of ca. 3.5% was at the highest temperature, 714 K, and the lowest pressure, 1 bar. At ambient temperature and 1 bar pressure the contribution was ca. 2%. At higher pressures the contribution is inversely proportionally smaller, and is completely negligible above 10 bar. Therefore, the diffusion controlled wall loss of methyl radical was neglected in our measurements.

The self-reactions of OH radicals and CH_3 radicals play significant role in the radical decays. In such cases, the rate constants resulting from the fits where all rate constants are allowed to vary are strongly correlated.[37] To circumvent this problem, the following approach was used. The experimental hydroxyl absorption profiles were converted into the hydroxyl concentration profiles on the basis of the measured absorption cross sections.[27] Then the hydroxyl concentration profiles were fitted using a smooth function with sufficient number of parameters to provide sufficient fitting flexibility. These profiles were then explicitly used in the methyl radical absorption profiles fitting using the SCIENTIST software, where unknown rate constant k_1 as well as the initial concentrations of methyl radicals were used as fitting parameters.

In addition to avoiding the large cross-correlation of the fitted rate constants, this approach also allowed for drastic reduction of the sensitivity of the fits to the rate constant of all other elementary reactions involving hydroxyl radical. As mentioned in ref 18, the ambiguity in the rate constant of reaction 13 (CH_2 + OH) might lead to a significant uncertainty in the determined rate constant of reaction 1 via the uncertainty in the apparent stoichiometric coefficient (up to a factor of 2), when OH absorption profiles are used for the determination of the rate constant of reaction 1. The explicit accounting for the OH concentration temporal profiles and using CH_3 absorption profiles in the fits completely alleviates this problem. Moreover, it leads to a large reduction of the sensitivity to the branching ratio in reaction 1.

To avoid complications associated with the cross-correlation of the rate constant of reaction 1 with the rate constant of reaction 7 (self-reaction of CH_3 radicals), this reaction was studied separately. The experiments were performed using acetone/water/He mixtures photolyzed at 193.3 nm. The absorption profiles at 216.4 nm of CH_3 were measured. The absorption cross sections of CH_3 (more exactly, the products of the absorption cross sections and the quantum yields of methyl radicals in the photolysis of acetone) were determined from the initial amplitudes of the absorption profiles and compared with the literature value[38] (see Supporting Information). The rate constants of CH_3 recombination reaction 7 were used as fitting parameters. The rate constants for reaction 1 (OH + CH_3 reaction) were determined from the outcomes of two experiments, where photolysis of the same mixture N_2O/H_2O/$(CH_3)_2CO$/He was used. In the first experiment the OH profile was recorded using hydroxyl lamp at 308 nm. In the second experiment, the monitoring light source was replaced with a xenon arc lamp, and absorption profiles were accumulated at 216.4 nm at the same experimental conditions. Sample absorption profiles obtained in this way are shown in Figure 1.

The procedure of the data processing then included two steps. In the first step the absorption profile at 308 nm was fitted by a two-exponential function with a free term (a five parameter fitting function) and then converted to the OH concentration profile. In the second step the hydroxyl concentration profile, $[OH](t)$, was transferred to the

dx.doi.org/10.1021/jp305070c | J. Phys. Chem. A 2012, 116, 8661−8670

SCIENTIST fitting model as an explicit concentration profile (i.e., the differential equation for [OH] was omitted). The numerical solutions of the residual set of ODE (for all transient spices except OH) with the proper initial conditions was used to fit the experimental absorption profile at 216.4 (where methyl is the major contributing species):

$$\mathrm{Abs}_{216.4}(t) = l(\sigma_{CH_3}[CH_3] + \sigma_{HONO}[HONO] + \sigma_{H_2O_2}[H_2O_2]) \quad \text{(E1)}$$

where l is the path length (10.13 cm). The absorption cross sections of CH_3 as well as the rate constant for the reaction of recombination of methyl radicals, k_7, were measured separately (Supporting Information). More exactly, the products of the apparent absorption cross sections of CH_3 radical at 216.4 nm and the branching ratios of the photolytic channel P2a in the photolysis of acetone at 193.3 nm (leading to two CH_3 radicals), $\sigma_{216.4}(CH_3) \times \phi_{P2a}$, as well as the product of the rate constants of methyl radical recombination and the branching ratios of the photolytic channel P2a, were measured. The branching ratio of the acetone photolysis channel leading to two CH_3 radicals at low pressures is $\phi_{P2a} = 0.95$.[33] The cross sections of HONO and H_2O_2 used were $\sigma_{216.4}(HONO) = 1.79 \times 10^{-18}$ cm^2 molecule^{-1} [39] and $\sigma_{216.4}(H_2O_2) = 2.96 \times 10^{-19}$ cm^2 molecule^{-1}.[40] We assumed the pressure independence of the cross sections of HONO and H_2O_2 in the data processing, as the concentrations of these species were very low. The rate constant k_1 and the initial concentration of CH_3 were used as fitting parameters. The results of the measurements are summarized in Table 1. It was assumed that the branching ratio of the acetone photolysis channel P2a is pressure independent ($\phi_{P2a} = 0.95$). However, at higher pressures, the yield of methyl radicals in the photolysis of acetone might be quenched. Measurements of the integral intensity of the CH_3 absorption spectra did suggest that such quenching (if exists), does not exceed 30% at 100 bar. The impact of possible pressure quenching of channel P2a on the rate constants returned by the fits was assessed. Decreasing the branching ratio ϕ_{P2a} by 30% lead to the increase of the returned rate constant k_1 by 5% at 294 K and 100 bar, and by 8% at 669 K and 100 bar. Such stability toward the methyl radical cross-section is again due to the explicit accounting for the hydroxyl concentration temporal profiles in the fits of the methyl radical absorption profiles. Morover, the uncertainty in the quantum yield of methyl radicals in photolysis of acetone at high pressures impacts both the measured absorption cross-section of methyl radicals at 216.4 nm and the recombination rate constant k_7. When *both* these parameters were increased by 30%, the impact on the returned rate constant k_1 did not exceed 0.5%.

There are two main contributions to the experimental errors. The first one is the uncertainties in the OH concentrations; the second one is the statistical error of the rate constants determination based on the CH_3 profiles. The first contribution is estimated as ±5%, evaluated from the data scatter as well as cross-section uncertainties in the ozone actinometry procedure. The second contribution depends on the signal/noise ratio in the CH_3 profiles and was varied within ±5 to ±20%. There are also minor contributions arising from the uncertainness in the rate constants of other reactions of CH_3 radical, mainly the $CH_3 + CH_3$ reaction (reaction 7). Numerical analysis of the sensitivity toward this rate constant in the typical experimental conditions resulted in $\delta(\ln k) = -0.34\ \delta(\ln k_{CH_3+CH_3})$. Assuming the accuracy of the rate constants of about ±20%, this adds about ±7% to the error. Considering these sources as independent, we estimate the uncertainties of the rate constants $\delta(\ln k) = (5^2 + 5^2 + 7^2)^{1/2} = 10\%$ for the good signal-to-noise ratio profiles (low pressures, low temperatures), and $\delta(\ln k) = (5^2 + 20^2 + 7^2)^{1/2} = 22\%$ for the lower signal-to-noise profiles (high pressure, high temperatures).

Pressure dependences of the rate constant of reaction 1 were measured at all temperatures of the study. The representative samples are shown in Figure 3. Over the pressure range studied

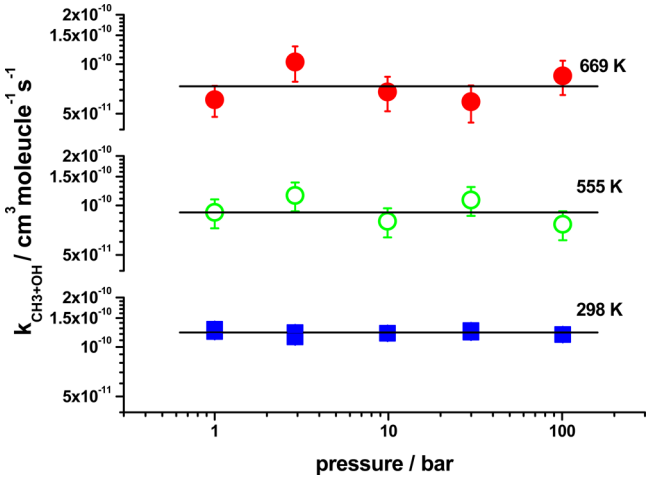

Figure 3. Pressure dependence of the rate constant of reaction 1 at different temperatures: filled squares, 298 K; open circles, 555 K; filled circles, 669 K.

(1−100 bar, He), no pressure dependence was observed at all temperatures of the study within the experimental error. Therefore, within the experimental error, the rate constants measured in this study are associated with the high pressure limit rate constant of reaction 1.

The temperature dependence of the rate constant k_1 is shown in Figure 4. It was fitted with a power function (solid line):

$$k_1 = (1.20 \pm 0.20) \times 10^{-10}(T/300)^{-0.49} \text{ cm}^3 \text{ molecule}^{-1} \text{ s}^{-1} \quad \text{(E2)}$$

In Figure 5 the results of the current study are plotted together with previous direct experimental determinations and theoretical studies. They appear to be in perfect agreement with the shock tube studies of Krasnoperov and Michael[18] as well as Vasudevan et al.[20] However, this observation could be misleading, because the shock tube studies were performed at much lower pressures (0.065−1.24 bar)[18] and (1.3−1.7 bar)[20] and are expected to be in the pressure falloff at this elevated temperatures.[20] However, a single experiment with pressure of ca. 5 bar did not reveal any increase in the rate constant at 1426 K compared with 1.2 bar.[20]

Jasper et al.[22] predicted ca. 2.1 times rate constant increase with pressure between 1 and 100 bar at 700 K, which was not observed in this work. The absolute value of the predicted rate constant by Jasper et al.[22] is in very good agreement with the current measurements. However, only very weak temperature dependence was predicted in this theoretical work. On the other hand, the temperature dependence measured in this work

dx.doi.org/10.1021/jp305070c | J. Phys. Chem. A 2012, 116, 8661−8670

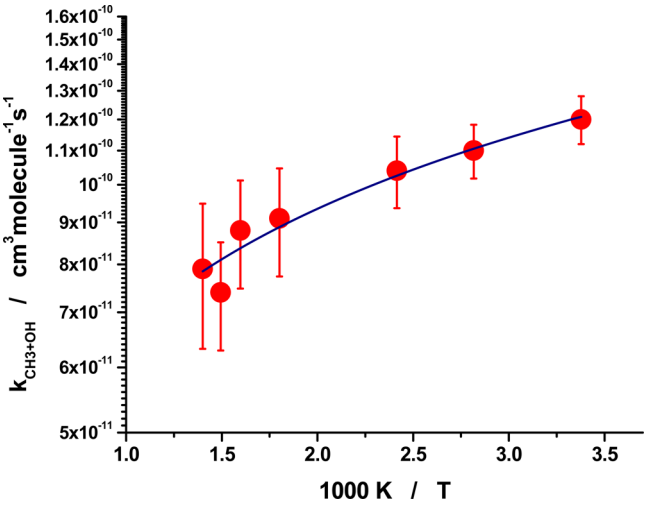

Figure 4. Pressure independent rate constant of reaction 1 as a function of temperature. The symbols are the average values at each temperature over the pressure range 1−100 bar (He). The solid line is the fit using the expression $k_1 = k_{1,300}(T/300)^n$.

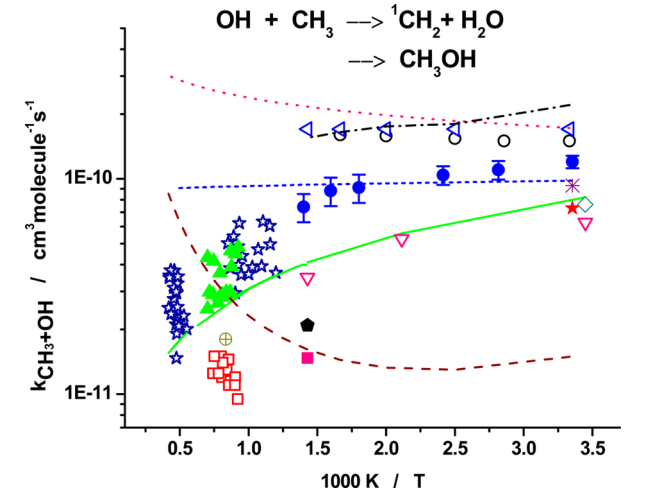

Figure 5. Arrhenius plot for the CH_3 + OH → products (reaction 1). Symbols: experimental studies. Lines: theoretical studies. Symbols: (●) this work; (☆) Krasnoperov and Michael;[18] (▲) Vasudevan et al.;[20] (□) Srinivasan et al.;[19] (⊗) Bott and Cohen;[17] (★) Deters et al.;[16] (∗) Sworski et al.;[6] (◇) Hughes et al.;[15] (○) Fagerstorm et al.;[8] (▽) Pereira et al.;[1] (■) Hompfer et al.;[11] (⬟) Hompfer et al.;[12] (◁) Oser et al.;[13] dashed line (− − −), Ing et al.;[21] short dashed line (---), Jasper et al.;[22] dotted line (···), Jordan et al.;[23] solid line (—), Pereira et al. high pressure extrapolation;[1] dash-dot-dash line (−·−), Xia et al.[2]

is in good agreement with that predicted by Pereira et al.,[1] although the predicted high pressure limit rate constant is ca. factor of 1.5−2 lower, than that measured in this work.

CONCLUSIONS

Reaction of methyl and hydroxyl radicals (reaction 1) was studied over extended temperature (294−714 K) and pressure (1−100 bar) ranges. The measured rate constants are independent of pressure within the pressure range of the study (1−100 bar, He) at all temperatures. The rate constant shows moderate negative temperature dependence, $k_1 \propto T^{-0.5}$.

ASSOCIATED CONTENT

Supporting Information

Absorption cross sections of acetone, the products of the apparent absorption cross sections of CH_3 radical at 216.4 nm and the branching ratios of the photolytic channel P2a in the photolysis of acetone at 193.3 nm (leading to two CH_3 radicals), $\sigma_{216.4}(CH_3) \times \phi_{P2a}$, kinetic parameters, the product of the rate constants of methyl radical recombination, and the branching ratios of the photolytic channel P2a, over the 1−100 bar and 298−714 K pressure and temperature ranges. This information is available free of charge via the Internet at http://pubs.acs.org.

AUTHOR INFORMATION

Corresponding Author

*FAX: (973)-596-8436. E-mail: krasnoperov@adm.njit.edu.

Notes

The authors declare no competing financial interest.

ACKNOWLEDGMENTS

This material is based upon work supported by the National Science Foundation under Grant No. CBET-0827398

REFERENCES

(1) Pereira, R. D. A.; Baulch, D. L.; Pilling, M. J.; Robertson, S. H.; Zeng, G. *J. Phys. Chem. A* **1997**, *101*, 9681−9693.
(2) Xia, W. S.; Zhu, R. S.; Lin, M. C.; Mebel, A. M. *Faraday Discuss.* **2001**, 191−205 ; discussion pp 255−174.
(3) Mirokhin, Y.; Mallard, G.; Westley, F.; Herron, J.; Frizzell, D.; Hampson, R. *NIST Standard Reference Database 17 - 2Q98 (Chemical Kinetics Database)*; National Institute of Standards and Technology: Gaithersburg, MD 20899, 1998.
(4) Ree, J.; Kim, Y. H.; Shin, H. K. *Int. J. Chem. Kinet.* **2011**, *43*, 455−466.
(5) Fockenberg, C.; Weston Ralph, E., Jr.; Muckerman James, T. *J. Phys. Chem. B* **2005**, *109*, 8415−8427.
(6) Sworski, T. J.; Hochanadel, C. J.; Ogren, P. J. *J. Phys. Chem.* **1980**, *84*, 129−134.
(7) Anastasi, C.; Beverton, S.; Ellermann, T.; Pagsberg, P. *J. Chem. Soc., Faraday Trans.* **1991**, *87*, 2325−2329.
(8) Fagerström, K.; Lund, A.; Mahmoud, G.; Jodkowski, J. T.; Ratajczak, E. *Chem. Phys. Lett.* **1993**, *204*, 226−234.
(9) Fagerstrom, K.; Lund, A.; Mahmoud, G.; Jodkowski, J. T.; Ratajczak, E. *Chem. Phys. Lett.* **1994**, *224*, 43−50.
(10) Grotheer, H. H.; Just, T. *Combust. Sci. Technol.* **1993**, *91*, 15−20.
(11) Humpfer, R.; Oser, H.; Grotheer, H.-H. *Int. J. Chem. Kinet.* **1995**, *27*, 577−595.
(12) Humpfer, R.; Oser, H.; Grotheer, H.-H.; Just, T. *Symp. (Int.) Combust., [Proc.]* **1994**, *25th*, 721−731.
(13) Oser, H.; Stothard, N. D.; Humpfer, R.; Grotheer, H. H. *J. Phys. Chem.* **1992**, *96*, 5359−5363.
(14) Oser, H.; Stothard, N. D.; Humpfer, R.; Grotheer, H. H.; Just, T. *Symp. (Int.) Combust., [Proc.]* **1992**, *24*, 597−604.
(15) Hughes, K. J.; Pereira, A. R.; Pilling, M. J. *Ber. Bunsen-Ges. Phys. Chem.* **1992**, *96*, 1352−1359.
(16) Deters, R.; Otting, M.; Wagner, H. G.; Temps, F.; Laszlo, B.; Dobe, S.; Berces, T. *Ber. Bunsen-Ges. Phys. Chem.* **1998**, *102*, 58−72.
(17) Bott, J. F.; Cohen, N. *Int. J. Chem. Kinet.* **1991**, *23*, 1017−1033.
(18) Krasnoperov, L. N.; Michael, J. V. *J. Phys. Chem. A* **2004**, *108*, 8317−8323.
(19) Srinivasan, N. K.; Su, M. C.; Michael, J. V. *J. Phys. Chem. A* **2007**, *111*, 3951−3958.
(20) Vasudevan, V.; Cook, R. D.; Hanson, R. K.; Bowman, C. T.; Golden, D. M. *Int. J. Chem. Kinet.* **2008**, *40*, 488−495.
(21) Ing, W.-C.; Sheng, C. Y.; Bozzelli, J. W. *Fuel Process. Technol.* **2003**, *83*, 111−145.

(22) Jasper, A. W.; Klippenstein, S. J.; Harding, L. B.; Ruscic, B. *J. Phys. Chem. A* **2007**, *111*, 3932−3950.
(23) Jordan, M. J. T.; Smith, S. C.; Gilbert, R. G. *J. Phys. Chem.* **1991**, *95*, 8685−8694.
(24) Grebenkin, S. Y.; Krasnoperov, L. N. *J. Phys. Chem. A* **2004**, *108*, 1953−1963.
(25) Krasnoperov, L. N.; Chesnokov, E. N.; Stark, H.; Ravishankara, A. R. *J. Phys. Chem. A* **2004**, *108*, 11526−11536.
(26) Krasnoperov, L. N.; Chesnokov, E. N.; Stark, H.; Ravishankara, A. R. *Proc. Combust. Inst.* **2005**, *30*, 935−943.
(27) Sangwan, M.; Chesnokov, E. N.; Krasnoperov, L. N. *J. Phys. Chem. A* **2012**, *116*, 6282−6294.
(28) Greenblatt, G. D.; Ravishankara, A. R. *J. Geophys. Res.* **1990**, *95*, 3539−3547.
(29) Sauder, D. G.; Stephenson, J. C.; King, D. S.; Casassa, M. P. *J. Chem. Phys.* **1992**, *97*, 952−961.
(30) Tanaka, N.; Takayanagi, M.; Hanazaki, I. *Chem. Phys. Lett.* **1996**, *254*, 40−46.
(31) Butler, J. E.; Talley, L. D.; Smith, G. K.; Lin, M. C. *J. Chem. Phys.* **1981**, *74*, 4501−4508.
(32) Cleveland, C. B.; Wiesenfeld, J. R. *J. Chem. Phys.* **1992**, *96*, 248−255.
(33) Lightfoot, P. D.; Kirwan, S. P.; Pilling, M. J. *J. Phys. Chem.* **1988**, *92*, 4938−4946.
(34) Micromath Scientific Software: Saint Louis, MO 63144.
(35) Parker, J. K.; Payne, W. A.; Cody, R. J.; Nesbitt, F. L.; Stief, L. J.; Klippenstein, S. J.; Harding, L. B. *J. Phys. Chem. A* **2007**, *111*, 1015−1023.
(36) Lewis, R. S.; Sander, S. P.; Wagner, S.; Watson, R. T. *J. Phys. Chem.* **1980**, *84*, 2009−2015.
(37) Krasnoperov, L. N.; Chesnokov, E. N. In *16th International Symposium on Gas Kinetics* Cambridge, U.K., 2000; Vol. Abstracts, p C8.
(38) Macpherson, M. T.; Pilling, M. J.; Smith, M. J. C. *J. Phys. Chem.* **1985**, *89*, 2268−2274.
(39) Schwarz, H. A.; Dodson, R. W. *J. Phys. Chem.* **1984**, *88*, 3643−3647.
(40) Vaghjiani, G. L.; Ravishankara, A. R. *J. Geophys. Res.* **1989**, *94*, 3487−3492.
(41) Vranckx, S.; Peeters, J.; Carl, S. *Phys. Chem. Chem. Phys.* **2010**, *12*, 9213−9221.
(42) Atkinson, R.; Baulch, D. L.; Cox, R. A.; Crowley, J. N.; Hampson, R. F.; Hynes, R. G.; Jenkin, M. E.; Rossi, M. J.; Troe, J. *Atmos. Chem. Phys.* **2004**, *4*, 1461−1738.
(43) Carl, S. A. *Phys. Chem. Chem. Phys.* **2005**, *7*, 4051−4053.
(44) Nishida, S.; Takahashi, K.; Matsumi, Y.; Taniguchi, N.; Hayashida, S. *J. Phys. Chem. A* **2004**, *108*, 2451−2456.
(45) Dunlea, E. J.; Ravishankara, A. R. *Phys. Chem. Chem. Phys.* **2004**, *6*, 2152−2161.
(46) Bahng, M.-K.; Macdonald, R. G. *J. Phys. Chem. A* **2007**, *111*, 3850−3861.
(47) Website: http://www.iupac-kinetic.ch.cam.ac.uk 2001, IUPAC Subcommittee on Gas Kinetic Data Evaluation.
(48) Bedjanian, Y.; Le Bras, G.; Poulet, G. *J. Phys. Chem. A* **1999**, *103*, 7017−7025.
(49) Srinivasan, N. K.; Su, M. C.; Sutherland, J. W.; Michael, J. V. *J. Phys. Chem. A* **2005**, *109*, 1857−1863.
(50) Tsang, W.; Hampson, R. F. *J. Phys. Chem. Ref. Data* **1986**, *15*, 1087−1279.
(51) Zellner, R.; Erler, K.; Field, D. *Symp. (Int.) Combust., [Proc.]* **1977**, *16*, 939−948.
(52) Atkinson, R.; Baulch, D. L.; Cox, R. A.; Hampson, R. F., Jr.; Kerr, J. A.; Troe, J. *J. Phys. Chem. Ref. Data* **1992**, *21*, 1125−1568.
(53) Fulle, D.; Hamann, H. F.; Hippler, H.; Troe, J. *J. Chem. Phys.* **1998**, *108*, 5391−5397.
(54) Tsang, W.; Hampson, R. F. *J. Phys. Chem. Ref. Data* **1986**, *15*, 1087−1279.
(55) Yamada, T.; Taylor, P. H.; Goumri, A.; Marshall, P. *J. Chem. Phys.* **2003**, *119*, 10600−10606.
(56) Jiménez, E.; Gierczak, T.; Stark, H.; Burkholder, J. B.; Ravishankara, A. R. *J. Phys. Chem. A* **2004**, *108*, 1139−1149.
(57) Keyser, L. F. *J. Phys. Chem.* **1988**, *92*, 1193−1200.
(58) Bardwell, M. W.; Bacak, A.; Teresa Raventos, M.; Percival, C. J.; Sanchez-Reyna, G.; Shallcross, D. E. *Phys. Chem. Chem. Phys.* **2003**, *5*, 2381−2385.
(59) Davies, J. W.; Green, N. J. B.; Pilling, M. J. *J. Chem. Soc., Faraday Trans.* **1991**, *87*, 2317−2324.